Terahertz control of air lasing

M. Clerici,[1,*] A. Bruhács,[2] D. Faccio,[3] M. Peccianti,[4] M. Spanner,[5] A. Markov,[2] B. E. Schmidt,[2,6] T. Ozaki,[2] F. Légaré,[2] F. Vidal,[2] and R. Morandotti[2,7,8,†]

[1]*School of Engineering, University of Glasgow, Glasgow, G12 8QQ, United Kingdom*
[2]*INRS-EMT, 1650 Blvd. Lionel-Boulet, Varennes, Québec J3X 1S2, Canada*
[3]*School of Physics and Astronomy, University of Glasgow, Glasgow G12 8QQ, United Kingdom*
[4]*Emergent Photonics Lab, Department of Physics and Astronomy, University of Sussex, Falmer Brighton, BN1 9QH, United Kingdom*
[5]*Steacie Institute for Molecular Sciences, National Research Council of Canada, Ottawa, Ontario K1A 0R6, Canada*
[6]*Few-Cycle Inc., 2890 Rue de Beaurivage, Montreal, Québec H1L 5W5, Canada*
[7]*ITMO University, St. Petersburg 199034, Russia*
[8]*Institute of Fundamental and Frontier Sciences, University of Electronic Science and Technology of China, Chengdu, China*

(Received 25 December 2018; published 2 May 2019)

The coherent emission from ionized nitrogen molecules is of interest for remote sensing and astronomical applications. To initiate the lasing process, we used an intense ultrashort near-infrared (NIR) pulse overlapped with a terahertz (THz) single-cycle pulse. We observed that coherent emission could be seeded and modulated by the amplitude of the THz field, which is the result of a combined effective second-order nonlinear polarization and the nonlinear effects induced by the NIR pump. Our results shed light on the role of intense transient fields in the coherent emission from photoexcited gas molecules.

DOI: 10.1103/PhysRevA.99.053802

One of the key phenomena accompanying the focusing of an intense laser pulse in air is the fluorescence from gas molecules [1–3]. Under appropriate excitation conditions, those molecules produce coherent radiation, which is appealing for standoff spectroscopy applications, especially when emitted in the opposite direction of the ionizing laser pulse [4,5]. Owing to nitrogen's abundance in our atmosphere, one of the most investigated effects has been the ultraviolet (UV) forward emission from photoexcited molecular nitrogen ions, first described as lasing by Luo and co-workers in 2003 [6]. A number of experiments report narrowband coherent emission at 391 nm and 428 nm, corresponding to the transitions $N_2^+[B\,^2\Sigma_u^+(\nu=0)] \rightarrow N_2^+[X\,^2\Sigma_g^+(\nu'=0,\ 1)]$ [see also Fig. 1(c) for potential energy diagrams]. Such observations show narrowband amplification at the frequencies corresponding to molecular transitions. Those are seeded, for instance, by harmonics of the near-infrared (NIR) pump pulse [7–9] or by white light [10], or self-seeded by the pump's supercontinuum itself [10–12]. Such reports have reinforced the idea that a lasing process is at the origin of the coherent emission. However, the mechanism responsible for the gain is still not fully understood, although it is likely that laser-driven couplings between electronic states in the ion [13,14] as well as rotational effects [15–21] play a role.

Here we report our experimental observation and analysis of the effect of a strong terahertz (THz) electric field on the coherent emission from photoexcited nitrogen ion molecules, as outlined in Figs. 1(a) and 1(b). We show a correlation between the THz field amplitude and the coherent emission at both 391 nm and 428 nm wavelengths. We interpret our results as a consequence of the THz electric field-induced symmetry breaking of the gas molecules. This, in turn, leads to a THz-controlled seeding of the coherent emission by means of the THz-induced second harmonic of the near-infrared pump pulse.

In our investigations, we used a single-cycle pulse at THz frequencies as a strong electric field. The THz transient was generated by the transverse photocurrents induced through gas ionization via a laser pulse at 1.8 μm carrier combined with its second harmonic. The THz pulse's bandwidth ($\sim$15 THz) was centered at $\simeq$ 5 THz, with a duration of $\simeq$ 90 fs, and a peak field amplitude of $\simeq$ 4 MV/cm. The THz field was recorded using air-biased coherent detection [22], as presented in Ref. [23]. The 790 nm NIR pump pulses were emitted by a Ti:Sapphire laser (Thales, France) at a 100 Hz repetition rate with a duration of 47 fs. The NIR and THz beams were focused at the same spatial coordinate. The experiment was conducted in a purged nitrogen atmosphere at a pressure of 1 atm. The THz beam was focused by a 5 cm diameter, off-axis, gold-coated parabolic mirror with 5 cm equivalent focal length. We measured the THz beam profile at the focus of the parabolic mirror using an infrared camera (PV-320, Electrophysics) and found the shape to be a Bessel-Gaussian, with a diameter of $\simeq$ 100 μm (full width at half maximum) and a Rayleigh range of $<$ 1 cm (see Ref. [24] for more details). The 790 nm beam was focused by a 150 mm focal length lens (with a resulting spot size of $\sim$26 μm) and overlapped to the THz beam through a hole in the focusing parabolic mirror, such that collinear propagation for the two beams could be achieved.

After passing through a polarizer, collimating lens, and a short-pass filter (Newport, BG40) the forward emitted UV radiation from the plasma was captured by an imaging

*matteo.clerici@glasgow.ac.uk
†morandotti@emt.inrs.ca

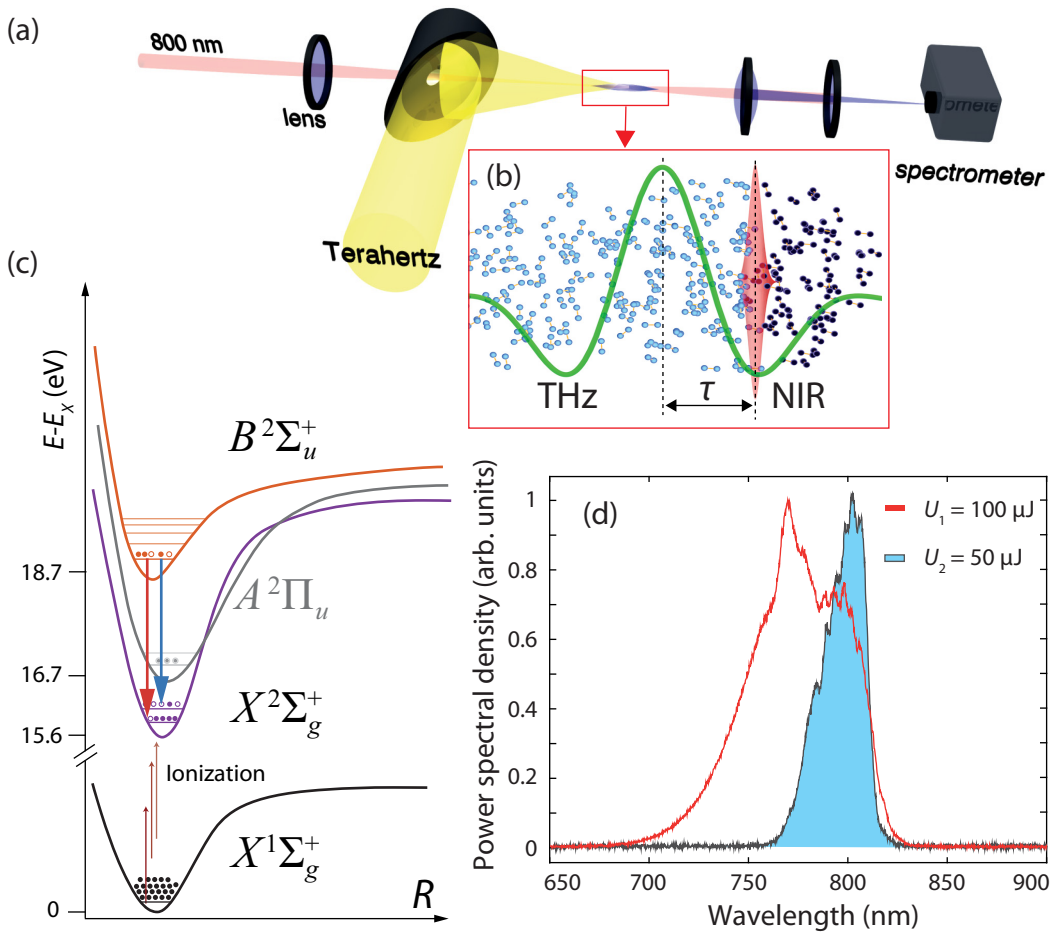

FIG. 1. THz-driven coherent emission in molecular nitrogen ions. (a) Sketch of the experimental setup. (b) Zoom of the near-infrared (NIR) pulse (pink-shaded) and THz transient (green line) interaction region. (c) Electronic states involved in molecular nitrogen ion coherent emission according to current literature [14]. N_2 undergoes multiphoton ionization (in the strong field regime) to N_2^+, distributed in X, A, or B. Red (blue) downward arrows represent the optical transitions at 391 nm (428 nm). (d) On-axis NIR pump spectra after the focus. The blue-shaded (red line) curves are for the low- (high-) energy pump cases, respectively. Both spectra are normalized to unity.

spectrometer (MS-260i, Newport) featuring a cooled charge-coupled device (620i, QSI). We compared NIR pump pulses with an energy of $U_1 \simeq 100\,\mu$J, which produce a visible plasma spark in the beam focus, with pulses of energy $U_2 \simeq 50\,\mu$J, which do not produce a visible plasma. Given our experimental conditions at the focus, the resulting peak intensities amount to $\sim 2.6 \times 10^{14}\,\mathrm{W/cm^2}$ and $\sim 1.3 \times 10^{14}\,\mathrm{W/cm^2}$, respectively, when not accounting for intensity clamping [25,26]. However, due to clamping effects, we assume the effective peak intensity to be below $1 \times 10^{14}\,\mathrm{W/cm^2}$ for both cases. Figure 1(d) shows the normalized spectra in the NIR region, where broadening and blueshifting of the input pump field is evident at high energies U_1.

When a portion of the THz field is overlapped in time with the NIR pump pulse, a broadband UV light at the second harmonic of the pump wavelength is produced. This is typically understood as a symmetry-breaking effect induced by the THz electric field resulting in a second-order nonlinear process, called Electric-Field-Induced Second Harmonic Generation (EFISH), and can be employed to measure the driving THz electric field [27–29]. Such an effect can be modeled as the combination of two sidebands of a third-order nonlinear optical interaction (namely, one sum-frequency and one difference-frequency generation process). The normalized UV spectra resulting from the interaction are shown in Fig. 2(a). It is clear that the only qualitative difference between the low- and high-energy cases is the emergence of narrowband spectral features at 391.5 nm and 427.8 nm. Figures 2(b) and 2(c) are close-ups of two relevant spectral windows between 386–396 nm and 418–429 nm, respectively. The panels (b) and (c) are normalized to the local maxima. In the absence of the THz field, only a low fluorescence signal can be observed, which is below the noise level of the measurement shown in Fig. 2.

We interpret these measurements as follows; on the one hand, the THz radiation induces an EFISH signal; see, e.g., the blue-shaded curve of Fig. 2(a). At sufficiently high NIR pulse energies, the nitrogen molecules start to be ionized, while the EFISH photons stimulate the emission from the gain established between the $B\,^2\Sigma_u^+ - X\,^2\Sigma_g^+$ states (in the following abbreviated as B and X). In turn, this leads to a narrowband amplification of the EFISH components at the frequency of the $v = 0 \rightarrow v' = 0,\ 1$ transitions. Recent literature confirms that coherent emission can be established

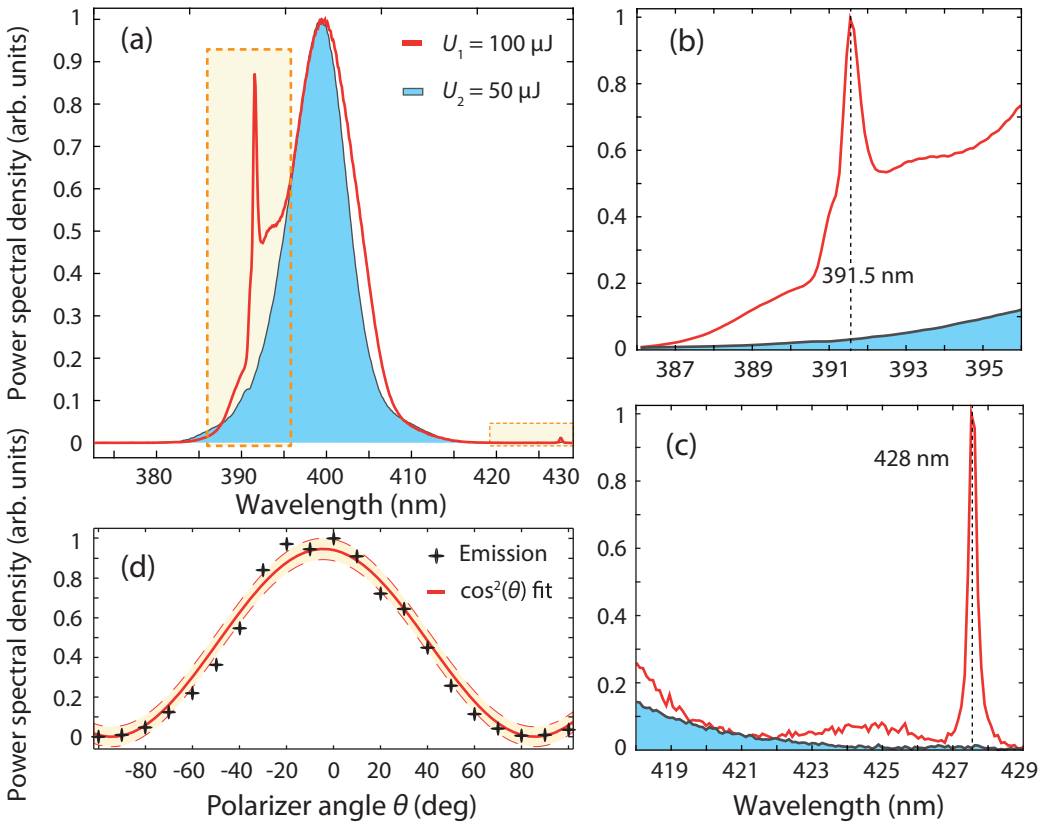

FIG. 2. Experimental results. (a) UV spectrum recorded in the far field of the THz and NIR pump interaction at $\tau = 0$. The solid red lines show the spectrum recorded for NIR pulses of energy 100 μJ. The blue-shaded curves depict the spectrum for 50 μJ pump pulses, i.e., for NIR pulses not inducing a visible plasma spark from gas ionization. The spectra are both normalized to unity. The yellow-shaded boxes identify the spectral region zoomed in panels (b) and (c). (d) Energy of the UV signal within a 1 nm region around the 391.5 nm emission line for different polarization angles. The red curve is the cosine square fit of the emission data points, with dashed red curves showing the 65% confidence bounds.

in conditions similar to those of our experiment for the case of high energy excitation (U_1) [6,12]. This narrowband amplification is evident from Figs. 2(b) and 2(c) and occurs close to the expected transition wavelengths 391.4 and 427.8 nm. To further distinguish the coherent emission from fluorescence, we characterized its polarization state. The measurements show that the emission at 391 nm is linearly polarized (the same for 427.8 nm; results not shown), featuring a polarization plane in common with the EFISH radiation. Figure 2(d) depicts the results of the polarization measurement performed on a narrowband spectral region (1 nm) around the 391.5 nm signal, overlaid with the expected cosine square fit. Blocking the THz pulse leads to a nearly zero background signal at the mentioned wavelength range. In summary, the first set of measurements indicates a possible role of the THz field as a seed for the nitrogen laser emission via the EFISH process.

In Fig. 2 we considered the UV radiation emitted by the THz-NIR interaction at a specific time delay ($\tau = 0$) between the two pulses. The zero delay was defined as the delay stage coordinate for which the incoherent EFISH signal was maximum. Next, we recorded the spectrogram of the UV radiation emitted by the two-pulse interaction, i.e., the spectrum as a function of the delay τ between such pulses, using a 15 fs step size for the time axis. The logarithm of the normalized spectrograms for U_1 and U_2 is shown in Figs. 3(a) and 3(b), respectively. The U_2 spectrogram closely resembles what is expected from four-wave mixing (FWM), as shown in the methods section of Ref. [30]. A faint signal, visible at 427.8 nm, indicates the presence of B nitrogen species, which are fluorescing to the unpopulated $v' = 1$ state of X. Around 391.5 nm we also observe a weak narrowband absorption signature, which further confirms the presence of ionized molecular nitrogen and shows that the $X(v' = 0)$ state is more populated than the upper $B(v = 0)$ state. In the high-energy case U_1, the large-scale features are still qualitatively similar to those acquired with lower pump energies; however, there is a clear indication of coherent emission at both 391.5 nm ($v = 0 \rightarrow v' = 0$) and 427.8 nm ($v = 0 \rightarrow v' = 1$) corresponding to two transitions from B to X.

Interestingly, the coherent emission at both wavelengths is delay-modulated and closely follows the amplitude of the measured THz electric field. We highlight this observation in Fig. 3(c), which depicts the UV power as a function of τ, within a 0.8 nm spectral band around 391 nm (red dot-dashed) and 428 nm (blue). The two curves are overlapped to $|E_{\mathrm{THz}}(\tau)|^2$ (black dashed), obtained from the electric field trace shown in Fig. 3(d). Details of the THz field employed in this experiment are reported in Ref. [30]. The modulation of

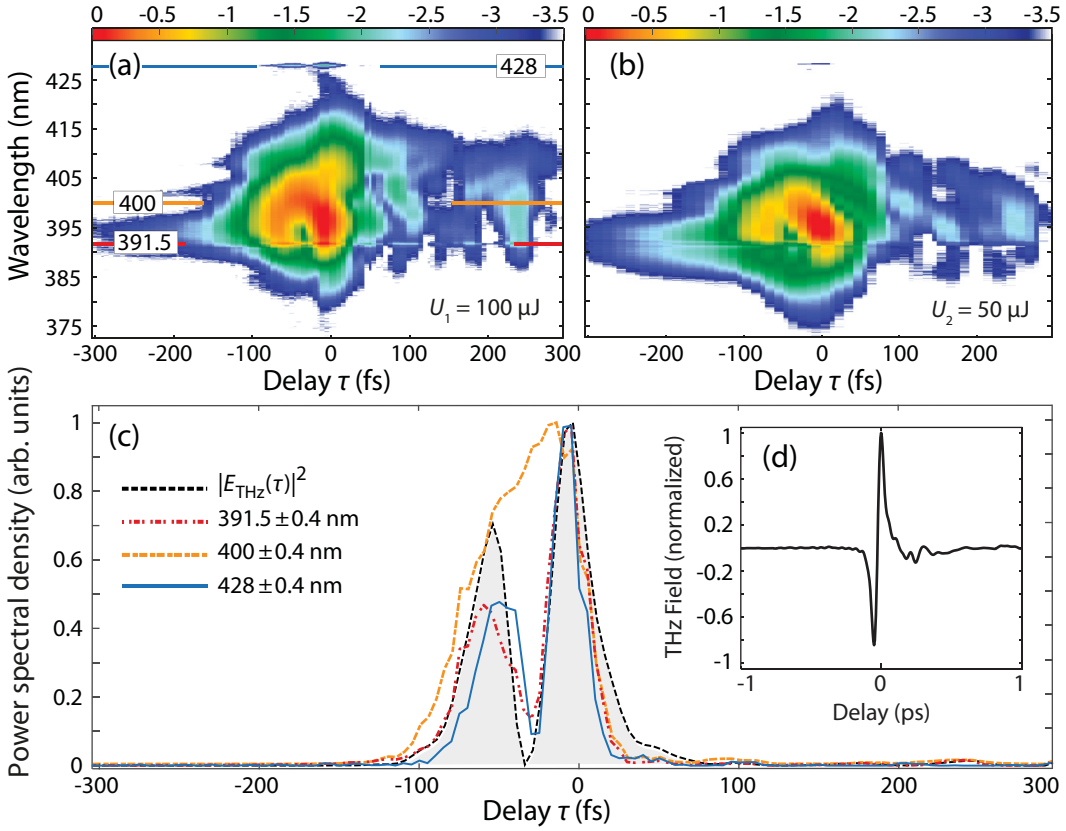

FIG. 3. Spectrograms of the nonlinear interaction. Panels (a) and (b) both show normalized data of the radiation emitted in the UV spectral region after the THz and NIR pump pulse interaction (the color scale represents the intensity in log scale). Data in (a) are recorded at a high NIR pump energy U1, and in (b) at a low-energy U2. The horizontal axis is the delay τ between the NIR pump and the THz single-cycle pulse. The thick horizontal segments in (a) identify the spectral regions of integration (0.8 nm) used to evaluate the traces reported in panel (c): the absolute value squared of the THz electric field (black dashed) is shown as a function of the temporal coordinate. It is overlapped to the integrated portion of the high-energy spectrogram signal around 391.5 nm (red), 400 nm (orange), and 428 nm (blue). All curves are normalized to their maximum value. (d) Measured THz field via the air-biased coherent detection method [22].

the 391 nm coherent emission can be interpreted as the consequence of the modulation of the seeding EFISH photons (see Appendix A). The EFISH process gives indeed rise to a delay-modulated signal close to the second-harmonic wavelength (395 nm) of the NIR pump pulse (790 nm); see Ref. [30]. Away from such a wavelength, the modulation visibility is expected to reduce and disappear quickly, as shown in the orange curve obtained by a lineout of the spectrogram in Fig. 3(c) at 400 nm. However, we experimentally observe that the 428 nm emission still follows the THz modulation with good visibility. This can be understood merely as a consequence of the pump pulse self-steepening induced by nonlinear propagation [3], thus leading to the formation of a shock front, which is confirmed by the broad blueshifted pump spectrum shown in Fig. 1(d).

We also note that pulse to pulse instabilities are evident from the discontinuities in the spectrogram, e.g., at ∼50 fs and 415 nm. Such discontinuities are not averaged by the 30 s long acquisition time in the spectrogram and, therefore, identify delay-spectral coordinates where the pulse instabilities play the most significant role in the nonlinear processes involved (pulse compression and wave mixing).

In order to simulate the generation and modulations of the UV seed, we model the EFISH process starting from the underpinning four-wave mixing, as detailed in Refs. [30,31]. This considers the nonlinearly emitted radiation as the scattering from a source with time-dependent polarization given by

$$P_{\mathrm{NL}}(t,\tau) \propto \chi^{(3)} E_{\mathrm{THz}}(t) E_p^2(t-\tau) \propto \chi^{(2)}_{\mathrm{eff}}(t) E_p^2(t-\tau), \quad (1)$$

$$\chi^{(2)}_{\mathrm{eff}}(t) \equiv \chi^{(3)} E_{\mathrm{THz}}(t), \quad (2)$$

where t is the time axis, and τ is the relative delay between the THz and the pump pulse, the latter being the driving pulse in our experiment. The sum and the difference frequency generation processes that are at the basis of the EFISH generation have, however, different efficiencies due to their respective longitudinal phases [32]. This can be phenomenologically modeled by introducing an imbalance parameter ϵ. Recalling Ref. [30], the resulting spectrogram amplitude can be described as

$$I(\tau,\omega) \propto \left| \int dt\, e^{i\omega t} \left[\left(\frac{1-\epsilon}{2} \right) E_{\mathrm{THz}}(t) + \left(\frac{1+\epsilon}{2} \right) E^*_{\mathrm{THz}}(t) \right] E_p^2(t-\tau) \right|^2, \quad (3)$$

where ω is the frequency coordinate of the Fourier transform. The characteristic horseshoe shape visible in the simulated

spectrogram shown in Fig. 4(a) can also be identified in the experimental results presented in Figs. 3(a) and 3(b). Figure 4(b) shows the result of lineouts at relevant wavelengths from the numerical spectrogram. It is important to note that our calculations also take into consideration the self-steepening of the pulse's trailing edge, as expected from nonlinear dynamics in the presence of ionization [3]. This type of temporal shaping leads to a broadening of the Fourier spectrum, which is also observed experimentally [see Fig. 1(d)] and thus gives rise to additional weaker seed modulations at 428 nm. In our simulations, the pump pulse duration was set to the experimentally measured value of 45 fs, while the imbalance parameter was tuned to $\epsilon = 0.6$ in order to match the experiments illustrated in Fig. 3(c). The experimental spectrogram presented in Fig. 3(a) shows that no coherent emission is observed unless the two pulses are temporally overlapped. In addition, the observed emission intensity modulation is almost thresholdless for the THz field amplitude. While several mechanisms could in principle lead to a THz-induced modulation of the air-laser emission (see Appendix B), we conclude that gain seeding in the plasma from the EFISH process is responsible for the observed effect.

In summary, we have demonstrated that THz radiation can control the coherent emission from molecular nitrogen ions in air via a nonlinear seeding mechanism, shedding new light on the instantaneous nature of the pump-induced gain process. In particular, we have shown that EFISH can seed the observed coherent emission. Although no coherent emission could be recorded counterpropagating the pump and THz direction, the proportionality of the UV signal to the square of the THz electric field could be further exploited as a means for remote THz detection. It remains an open question whether a strong THz field could directly affect the mechanism leading to the observed gain in photoexcited nitrogen, e.g., via the control of the molecular rotational states.

All data relative to this paper are available at Ref. [33].

The authors would like to gratefully acknowledge NSERC (the National Science and Engineering Research Council) in Canada and the MEES (the Ministère de l'Éducation et de l'Enseignement Supérieur) in Quebec. M.C. acknowledges the support from the United Kingdom Research and Innovation (UKRI), the Engineering and Physical Sciences Research Council (EPSRC), and Innovate UK (UKRI Innovation Fellowship EP/S001573/1 and Innovate UK/EPSRC EP/R043299/1). A.B. acknowledges support from Le Fonds Quebecois de la Recherche sur la Nature et les Technologies, through the Post-Doctoral Fellowship Program (File 206944). D.F. acknowledges financial support from the European Research Council under the European Union's Seventh Framework Program (FP/2007–2013)/ERC GA 306559 and EPSRC (U.K., Grant EP/J00443X/1). M.P. acknowledges that this project has received funding from the European Research Council (ERC) under the European Union's Horizon 2020 research and innovation program Grant agreement 725046. R.M. further acknowledges support by the Government of the Russian Federation through the ITMO Fellowship and Professorship Program (grant 074-U 01) and from the 1000 Talents Sichuan Program. The authors would like to thank S.-L. Chin, J.-C. Diels, L. Arissian, and A. Baltuška for enlightening discussions. Finally, the authors would like to thank the team of technicians at the INRS-EMT Advanced Laser Light Source for their kind support.

M.C. and A.B. equally contributed to the work.

APPENDIX A: GAUSSIAN PUMP MODEL FOR FOUR-WAVE MIXING LEADING TO EFISH

Figure 5 and Ref. [30] both show that EFISH modulated seeding using a simple temporal Gaussian pump pulse (790 nm, 45 fs) is achievable via four-wave mixing (FWM) mostly below ~400 nm and, in particular, not at 428 nm. In contrast, our experimental results reveal a seed modulation at 428 nm.

As presented in Fig. 4, we include a shock front term in our model, which ultimately leads to a spectral broadening of the driving pump pulse and enhanced modulation at the spectral wings. Note that all simulations include a fitted linear chirp in the carrier of the pump pulse which spans the entire measured bandwidth. We found that the implementation of this linear

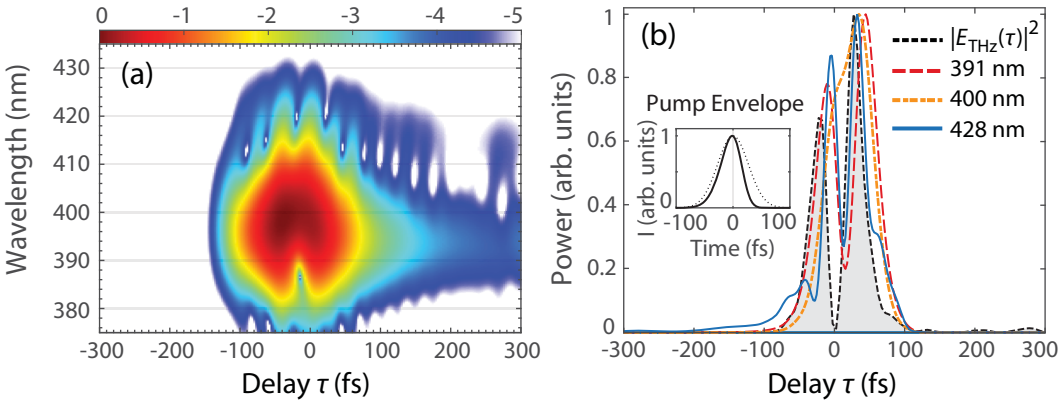

FIG. 4. Simulated four-wave mixing spectrograms of the nonlinear process. Panel (a) shows the interaction between a shock front (asymmetric) Gaussian pump pulse (centered at 790 nm, 45 fs in duration) with the measured THz pulse waveform. The color bar indicates the normalized intensity in arbitrary logarithmic units. Spectral lineouts are shown in panel (b) and overlaid with the measured THz waveform. Panel (b) displays modulations at 391 nm (red dashed curve), as well as 428 nm (blue), while no modulations occur at 400 nm (orange dot-dashed curve). The inset in panel (b) displays the simulated pump pulse's temporal profile compared to that of a symmetric Gaussian pulse.

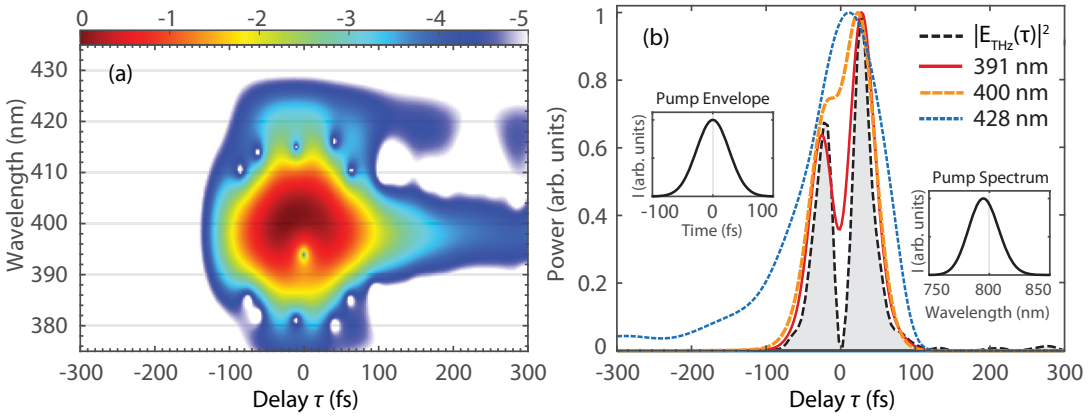

FIG. 5. Simulated four-wave mixing spectrogram of the nonlinear interaction. Panel (a) shows the interaction of the pump pulse (centered at 790 nm, 45 fs in duration, and featuring a Fourier-limited bandwidth) with the measured THz pulse waveform, assuming a symmetric, Fourier-limited, Gaussian profile. The color bar indicates the normalized intensity in arbitrary logarithmic units. Spectral lineouts are shown in panel (b) and overlaid with the measured THz waveform (dashed black line). Panel (b) displays modulations only at 391 nm (red curve) and does not feature modulations either at 400 nm (orange dashed curve) or at 428 nm (blue dashed curve), thus contradicting our experimental results. The two insets in panel (b), left and right, display the pump pulse's temporal and spectral profiles, respectively, under the simplified assumption above.

chirp leads to an improved fit in the numerically calculated FWM amplitudes $I(\tau, \omega)$, particularly in the ratio between the two lobes of the FWM interaction.

APPENDIX B: RULING OUT ALTERNATIVE MECHANISMS THAT COULD LEAD TO THZ-INDUCED MODULATION OF COHERENT EMISSION

In what follows, we discuss the mechanisms that may enable the THz electric field to modulate emissions from the nitrogen cation N_2^+.

(a) Inelastic collisions. It is known that strong THz radiation can accelerate free carriers due to its large ponderomotive energy. The heated electron gas could then transfer energy to high-lying nitrogen states [i.e., $N_2(C^3\Pi_\pi)$] via inelastic collisions, providing a pathway to increased ionization. Liu and co-workers have indeed observed this process, reporting an enhancement in the molecular nitrogen fluorescence (captured perpendicular to the propagation direction) in the presence of both a two-color generated plasma and a strong THz field [34,35]. Specifically, they have shown how this process leads to a fluorescence increase proportional to $\Delta FL(\tau) \propto \int_{\tau+t_\phi}^{\infty} E_{\mathrm{THz}}^2(t)\ dt$, where t_ϕ is a phase delay induced by the plasma formation dynamics. In stark contrast to this observation, our experiment shows that the coherent radiation emitted in the forward direction behaves as a function of the instantaneous THz electric field: $I_{\mathrm{Laser}}^{N_2^+}(\tau) \propto |E_{\mathrm{THz}}(t)|^2$, as seen in Fig. 3(c). In addition, the stepwise energy transfer mechanism suggested in Ref. [35] would lead at best to an enhancement in the ionization yield of the X state, and not in B or $A^2\Pi_u^+$. Also, Liu *et al.* do not report significant THz-modulated enhancement of the $B \rightarrow X$ ($0 \rightarrow 0$ and $0 \rightarrow 1$) transitions in the forward direction. This suggests that the mechanism underpinning our observations is of a different nature [34].

(b) Molecular rotation effects. A number of recent works address processes involving the rotational alignment of diatomic molecules under strong nonresonant fields in the presence of a resonant THz field [36–38]. Indeed, a strong THz field is capable of aligning and orienting molecules [39,40], and recently, field-free alignment of neutral N_2 with single-cycle THz fields has been observed [41]. However, we exclude this to be at the origin of the coherent emission observed in our work, as nonadiabatic molecular alignment is comparatively slow with respect to the gain dynamics observed in N_2^+ air lasing [21]. Furthermore, the molecular orientation is reportedly a function of the THz intensity profile, rather than the instantaneous electric field. Hence no modulation is expected at the THz carrier frequency.

[1] A. Talebpour, M. Abdel-Fattah, and S. Chin, Opt. Commun. **183**, 479 (2000).
[2] A. Talebpour, M. Abdel-Fattah, A. D. Bandrauk, and S. L. Chin, Laser Phys. **11**, 68 (2001).
[3] A. Couairon and A. Mysyrowicz, Phys. Rep. **441**, 47 (2007).
[4] M. N. Shneider, A. Baltuška, and A. M. Zheltikov, J. Appl. Phys. **110**, 083112 (2011).
[5] D. Kartashov, S. Ališauskas, G. Andriukaitis, A. Pugžlys, M. Shneider, A. Zheltikov, S. L. Chin, and A. Baltuška, Phys. Rev. A **86**, 033831 (2012).
[6] Q. Luo, W. Liu, and S. L. L. Chin, Appl. Phys. B Lasers Opt. **76**, 337 (2003).
[7] J. Yao, B. Zeng, H. Xu, G. Li, W. Chu, J. Ni, H. Zhang, S. L. Chin, Y. Cheng, and Z. Xu, Phys. Rev. A **84**, 051802 (2011).

[8] J. Ni, W. Chu, H. Zhang, C. Jing, J. Yao, H. Xu, B. Zeng, G. Li, C. Zhang, S. L. Chin, Y. Cheng, and Z. Xu, Opt. Express **20**, 20970 (2012).
[9] J. Yao, G. Li, C. Jing, B. Zeng, W. Chu, J. Ni, H. Zhang, H. Xie, C. Zhang, H. Li, H. Xu, S. L. Chin, Y. Cheng, and Z. Xu, New J. Phys. **15**, 023046 (2013).
[10] T.-J. Wang, J.-F. Daigle, J. Ju, S. Yuan, R. Li, and S. L. Chin, Phys. Rev. A **88**, 053429 (2013).
[11] Y. Liu, Y. Brelet, G. Point, A. Houard, and A. Mysyrowicz, Opt. Express **21**, 22791 (2013).
[12] W. Chu, G. Li, H. Xie, J. Ni, J. Yao, B. Zeng, H. Zhang, C. Jing, H. Xu, Y. Cheng, and Z. Xu, Laser Phys. Lett. **11**, 015301 (2014).
[13] H. Xu, E. Lötstedt, A. Iwasaki, and K. Yamanouchi, Nat. Commun. **6**, 8347 (2015).
[14] J. Yao, S. Jiang, W. Chu, B. Zeng, C. Wu, R. Lu, Z. Li, H. Xie, G. Li, C. Yu, Z. Wang, H. Jiang, Q. Gong, and Y. Cheng, Phys. Rev. Lett. **116**, 143007 (2016).
[15] A. Azarm, P. Corkum, and P. Polynkin, Phys. Rev. A **96**, 051401 (2017).
[16] H. Zhang, C. Jing, J. Yao, G. Li, B. Zeng, W. Chu, J. Ni, H. Xie, H. Xu, S. L. Chin, K. Yamanouchi, Y. Cheng, and Z. Xu, Phys. Rev. X **3**, 041009 (2013).
[17] B. Zeng, W. Chu, G. Li, J. Yao, H. Zhang, J. Ni, C. Jing, H. Xie, and Y. Cheng, Phys. Rev. A **89**, 042508 (2014).
[18] L. Arissian, B. Kamer, and A. Rasoulof, Opt. Commun. **369**, 215 (2016).
[19] B. Kamer, J. C. Diels, and L. Arissian, Ultrafast Spectroscopy Using Coherent Wavepackets, in *OSA CLEO Conference Papers*, OSA Technical Digest (online) (Optical Society of America, 2017), p. JTh2A.17.
[20] D. Kartashov, S. Haessler, S. Ališauskas, G. Andriukaitis, A. Pugžlys, A. Baltuška, J. Möhring, D. Starukhin, M. Motzkus, A. M. Zheltikov, M. Richter, F. Morales, O. Smirnova, M. Y. Ivanov, and M. Spanner, Transient Inversion in Rotationally Aligned Nitrogen Ions in a Femtosecond Filament, in *Research in Optical Sciences*, OSA Technical Digest (online) (Optical Society of America, Washington, DC, 2014), p. HTh4B.5.
[21] M. Lei, C. Wu, A. Zhang, Q. Gong, and H. Jiang, Opt. Express **25**, 4535 (2017).
[22] N. Karpowicz, J. Dai, X. Lu, Y. Chen, M. Yamaguchi, H. Zhao, X.-C. Zhang, L. Zhang, C. Zhang, M. Price-Gallagher, C. Fletcher, O. Mamer, A. Lesimple, and K. Johnson, Appl. Phys. Lett. **92**, 011131 (2008).
[23] M. Clerici, M. Peccianti, B. E. Schmidt, L. Caspani, M. Shalaby, M. Giguère, A. Lotti, A. Couairon, F. Légaré, T. Ozaki, D. Faccio, and R. Morandotti, Phys. Rev. Lett. **110**, 253901 (2013).
[24] M. Clerici, D. Faccio, L. Caspani, M. Peccianti, E. Rubino, L. Razzari, F. Légaré, T. Ozaki, and R. Morandotti, Opt. Lett. **38**, 1899 (2013).
[25] S. L. Chin, T.-J. Wang, C. Marceau, J. Wu, J. S. Liu, O. Kosareva, N. Panov, Y. P. Chen, J.-F. Daigle, S. Yuan, A. Azarm, W. W. Liu, T. Seideman, H. P. Zeng, M. Richardson, R. Li, and Z. Z. Xu, Laser Phys. **22**, 1 (2012).
[26] P. P. Kiran, S. Bagchi, C. L. Arnold, S. R. Krishnan, G. R. Kumar, and A. Couairon, Opt. Express **18**, 21504 (2010).
[27] R. S. Finn and J. F. Ward, Phys. Rev. Lett. **26**, 285 (1971).
[28] C. Ohlhoff, C. Meyer, G. Lüpke, T. Löffler, T. Pfeifer, H. G. Roskos, and H. Kurz, Appl. Phys. Lett. **68**, 1699 (1996).
[29] A. Nahata and T. F. Heinz, Opt. Lett. **23**, 67 (1998).
[30] M. Clerici, D. Faccio, L. Caspani, M. Peccianti, O. Yaakobi, B. E. Schmidt, M. Shalaby, F. Vidal, F. Légaré, T. Ozaki, and R. Morandotti, New J. Phys. **15**, 125011 (2013).
[31] R. W. Boyd, *Nonlinear Optics*, third ed. (Academic Press, Inc., Orlando, FL, USA, 2008).
[32] X. Lu, N. Karpowicz, and X.-C. Zhang, J. Opt. Soc. Am. B **26**, A66 (2009).
[33] M. Clerici *et al.*, Research data for "Terahertz control of air lasing," 10.5525/gla.researchdata.777 (2019).
[34] J. Liu and X.-C. Zhang, Phys. Rev. Lett. **103**, 235002 (2009).
[35] J. Liu, J. Dai, S. L. Chin, and X. Zhang, Nat. Photonics **4**, 627 (2010).
[36] H. P. Dang, S. Wang, W. S. Zhan, X. Han, and J. B. Zai, Laser Phys. **25**, 075301 (2015).
[37] Y. Huang, T. Xie, J. Li, J. Yu, and S.-L. Cong, Laser Phys. **24**, 016002 (2014).
[38] C.-C. Shu and N. E. Henriksen, Phys. Rev. A **87**, 013408 (2013).
[39] S. Fleischer, R. W. Field, and K. A. Nelson, Phys. Rev. Lett. **109**, 123603 (2012).
[40] K. Kitano, N. Ishii, and J. Itatani, Phys. Rev. A **84**, 053408 (2011).
[41] M. Shalaby and C. P. Hauri, Appl. Phys. Lett. **106**, 181108 (2015).